Switching the direction of spin accumulation in the spin Hall effect of light by adjusting the optical axis of an uniaxial crystal*

Tang Ming(唐 明), Zhou Xin-Xing(周新星), Xiao Zhi-Cheng(肖志成),
Luo Hai-Lu(罗海陆)†, and Wen Shuang-Chun(文双春)

Key Laboratory for Micro-/Nano-Optoelectronic Devices of Ministry of Education, School of Information Science and Engineering, Hunan University, Changsha 410082, *China*

(Received 31 October 2012; revised manuscript received 12 November 2012)

We theoretically and experimentally investigate a switchable spin Hall effect (SHE) of light in reflection near the Brewster angle at an air–uniaxial crystal interface. We find a large transverse spin splitting near the Brewster angle, whose sign can be altered by rotating the optical axis. As an analogy of the SHE in an electronic system, a switchable spin accumulation in the SHE of light is detected. We are able to switch the direction of the spin accumulation by adjusting the optical axis angle of the uniaxial crystal. These findings may give opportunities for photon spin manipulating and developing a new generation of nano-photonic devices.

Keywords: spin Hall effect of light, spin accumulation, uniaxial crystal, transverse displacement

PACS: 41.20.Jb, 42.25.Dd, 42.79.–e **DOI:** 10.1088/1674-1056/22/3/034101

1. Introduction

The spin Hall effect (SHE) of light is the spin-dependent transverse shift of a wave packet, which can be regarded as the photonic version of the SHE in electronic systems, where the spin photons play the role of the spin charge, and the refractive index gradient plays the role of the electric potential gradient.[1–3] More recently, there has been keen interest in the SHE of light both in theory[4–9] and in experiments.[10–17] The SHE of light may open new opportunities for manipulating photon spins and developing new generations of all-optical devices as the counterparts of recently presented spintronic devices. The generation, manipulation, and detection of spin-polarized electrons in semiconductors define the main challenges of spin-based electronics.

Effectively switching the directions of spin accumulation in the SHE of light for possible applications is worthy of study. It was found that the directions of the spin currents can be switched by rotating the polarization plane of the exciting light in a semiconductor micro-cavity.[18] In our previous paper,[19] we demonstrated an enhanced and switchable SHE of light near the Brewster angle on reflection at an air–isotropic medium interface. In that paper, we found that the directions of spin accumulations in the SHE of light can be switched by slightly adjusting the incident angle. However, the refracted angle changes and the transmission coefficients decrease accordingly as the incident angle increases. Hence, it is disadvantageous to potential applications of nanophotonic devices.

In this paper, we propose a novel approach to switch the directions of spin accumulation in the SHE of light without altering the incident angle. When the beam incidents away from the Brewster angle, the transverse displacements between the two spin components are small.[15] However, we find a large transverse spin splitting near the Brewster angle on reflection. Moreover, the Brewster angle of an anisotropic medium can be varied by rotating the optical axis of the anisotropic medium. Now a question naturally arises: can we utilize the anisotropic medium to switch the directions of spin accumulation in the SHE of light near the Brewster angle? In this paper, we demonstrate that we can switch the directions of spin accumulation in the SHE of light by altering the optical axis angle. And we also theoretically and experimentally confirm that the transverse displacements can be amplified near the Brewster angle at an air–uniaxial crystal interface.

2. Theoretical analysis

We begin by studying a linearly polarized light beam impinging upon a planar interface that is composed of air and an uniaxial crystal sample (YVO_4). When reflected at the interface, the linearly polarized incident beam splits into two spin components that acquire opposite lateral displacements perpendicular to the incident plane: components parallel (δ_+^{H}, left-handed circularly polarized) and antiparallel (δ_-^{H}, right-handed circularly polarized) to the central wave vector, as shown in Fig. 1. We use a laboratory Cartesian frame (x, y, z) attached to the interface and the coordinate systems of the individual beams, where (x_{i}, y_{i}, z_{i}) and (x_{r}, y_{r}, z_{r}) are attached to the incident and the reflected beams, respectively. The z_{i}

*Project supported by the National Natural Science Foundation of China (Grants Nos. 61025024 and 11074068) and the Hunan Provincial Natural Science Foundation of China (Grant No. 12JJ7005).

†Corresponding author. E-mail: hailuluo@hnu.edu.cn

© 2013 Chinese Physical Society and IOP Publishing Ltd

and z_r axes attach to the directions of the central wave vectors of the incident and the reflected beams as determined by the Snell's law, respectively.

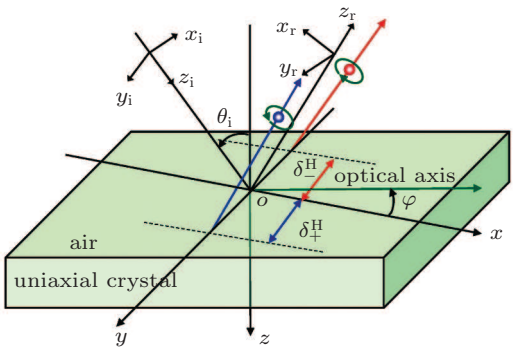


Fig. 1. (color online) Schematic diagram of SHE of light at the air–uniaxial crystal interface, where $\delta_\pm^H$ denotes the displacements of left-circularly polarized and right-circularly polarized spin components. Here, θ_i is the incident angle, subscripts i and r correspond to incident light and reflected light, respectively.

In the spin basis set, the incident angular spectrum can be written as $\tilde{\boldsymbol{E}}_i^H = (\tilde{\boldsymbol{E}}_{i+} + \tilde{\boldsymbol{E}}_{i-})/\sqrt{2}$, $\tilde{\boldsymbol{E}}_i^V = i(\tilde{\boldsymbol{E}}_{i-} - \tilde{\boldsymbol{E}}_{i+})/\sqrt{2}$. Here, H and V represent the horizontal and vertical polarizations, respectively. The positive and negative signs denote the left and right circularly polarized components, respectively.[20] The incident monochromatic Gaussian beam can be formulated as a localized wave packet whose spectrum is arbitrarily narrow, and can be written as

$$\tilde{\boldsymbol{E}}_{i\pm} = (\boldsymbol{e}_{ix} \pm i\boldsymbol{e}_{iy}) \frac{w_0}{\sqrt{2\pi}} \exp\left[-\frac{w_0^2(k_{ix}^2 + k_{iy}^2)}{4}\right], \quad (1)$$

where w_0 is the beam waist. In the spin basis, $\tilde{\boldsymbol{E}}_r^H = (\tilde{\boldsymbol{E}}_{r+} + \tilde{\boldsymbol{E}}_{r-})/\sqrt{2}$ and $\tilde{\boldsymbol{E}}_r^V = i(\tilde{\boldsymbol{E}}_{r-} - \tilde{\boldsymbol{E}}_{r+})/\sqrt{2}$, where $\tilde{\boldsymbol{E}}_{r+} = (\boldsymbol{e}_{rx} + i\boldsymbol{e}_{ry})\tilde{\xi}_r/\sqrt{2}$, $\tilde{\boldsymbol{E}}_{r-} = (\boldsymbol{e}_{rx} - i\boldsymbol{e}_{ry})\tilde{\xi}_r/\sqrt{2}$, with $\tilde{\xi}_r$ being obtained from Eq. (1) and boundary conditions $k_{ix} = -k_{rx}$ and $k_{iy} = k_{ry}$.

Consider an incident beam of H polarization, we can obtain the expression for the reflected angular spectrum

$$\tilde{\boldsymbol{E}}_r^H = \frac{r_p}{\sqrt{2}}[(1 - i\eta k_{ry})\tilde{\boldsymbol{E}}_{r+} + (1 + i\eta k_{ry})\tilde{\boldsymbol{E}}_{r-}], \quad (2)$$

where $\eta = (1 + r_s/r_p)\cot\theta_i/k_0$, and r_p and r_s denote the Fresnel reflection coefficients for the p and s components of the wave, respectively. They can be expressed as $r_s = (k_0\cos\theta_i - k_z^s)/(k_0\cos\theta_i + k_z^s)$, $r_p = (k_0\cos\theta_i - \chi)/(k_0\cos\theta_i + \chi)$, where k_0 is the wave vector in the air; θ_i denotes the incident angle; k_z^s and k_z^p are the wave vectors in the uniaxial crystal for the s and p components of the wave, respectively; n_e and n_o are the refractive indexes for the ordinary and the extraordinary rays, respectively; $\chi = [(n_o^2 - n_e^2)\cos\varphi(-k_z^p\cos\varphi + k_x\sin\varphi) + k_z^p n_o^2]/(n_e^2 n_o^2)$; and φ represents the angle between the optical axis of the uniaxial crystal and the x axis. The complex amplitude of the reflected beam can be conveniently expressed as

$$\boldsymbol{E}_{r\pm}(x_r, y_r, z_r) = \int dk_{rx}dk_{ry}(1 \mp \eta k_{ry})\tilde{\boldsymbol{E}}_{r\pm}(k_{rx}, k_{ry}) \times \exp[i(k_{rx}x_r + k_{ry}y_r + k_{rz}z_r)], \quad (3)$$

where $k_{rz} = \sqrt{k_r^2 - (k_{rx}^2 + k_{ry}^2)}$.

Here, we investigate the spin-dependent displacements of the reflected light induced by the SHE of light both theoretically and experimentally. At any given plane $z_r = \text{const.}$, the transverse displacement of the field centroid compared to the geometrical-optics prediction is given by

$$\delta_\pm^H = \frac{\int\int y_r I_\pm^H(x_r, y_r, z_r)\,dx_r dy_r}{\int\int I_\pm^H(x_r, y_r, z_r)\,dx_r dy_r}. \quad (4)$$

The intensity distribution of the beam is closely linked to the longitudinal momentum current $I(x_r, y_r, z_r) \propto \boldsymbol{P}_r \cdot \boldsymbol{e}_{rz}$. The time-averaged linear momentum density associated with the electromagnetic field can be shown to be $\boldsymbol{P}_r \propto \mathrm{Re}[\boldsymbol{E}_r \times \boldsymbol{H}_r^*]$, where the magnetic field can be obtained by $\boldsymbol{H}_r = -ik_r^{-1}\nabla \times \boldsymbol{E}_r$.

3. Experimental results and discussion

To measure the transverse displacements, we use the signal enhancement technique[3] known as weak measurements.[21,22] The experimental setup is shown in Fig. 2. A Gaussian beam generated by an He–Ne laser passes through a short focal length lens (Lens1) and a polarizer (GLP1) to produce an initially polarized focused beam. The He–Ne laser operating at a wavelength of 632.8 nm with a minimum waist of 0.98 mm is focused by a lens with focal length $f_1 = 50$ mm, a waist of $w_0 = 18.66$ μm is produced. The beam splits into two spin components when reflected at the interface of YVO_4 with the size of 20 mm × 20 mm × 10 mm. The refractive index for the ordinary and the extraordinary rays are $n_o = 1.992$ and $n_e = 2.218$ at 632.8 nm, respectively. The crystal is mounted on a rotation stage which allows for the

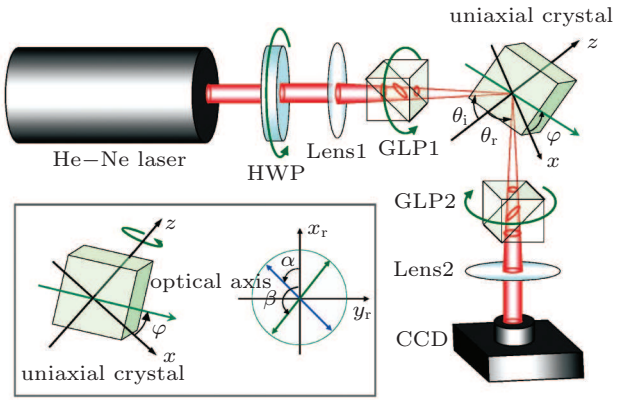


Fig. 2. (color online) Experimental setup for characterizing the SHE of light in reflection at the interface of YVO_4 crystal. The laser is a linearly polarized He–Ne laser at 632.8 nm, 17 mW (Thorlabs HRP170); HWP is a half-wave plate for attenuating the intensity after GLP1 to prevent the CCD from saturating; Lens1 and Lens2 are lenses with effective focal lengths $f_1 = 50$ mm and $f_2 = 250$ mm, respectively; Uniaxial crystal YVO_4 is the experimental sample; GLP1 and GLP2 are Glan laser polarizers; and CCD is a charge-coupled device (Coherent LaserCam HR).

precise control of the incident angle θ_i. The incident beam is preselected in the H polarization state ($\alpha = 0°$) by GLP1, and then postselected ($\beta = \pi/2 + \Delta$) by GLP2 in the polarization state with $\boldsymbol{v} = \sin\Delta \boldsymbol{e}_{rx} + \cos\Delta \boldsymbol{e}_{ry}$. The relevant amplitude of the reflected field at the plane of z_r can be obtained as $\boldsymbol{v} \cdot \boldsymbol{E}_r$. The amplified displacement of field centroid δ_w at the CCD is much larger than the original displacement $|\delta_{\pm}^H|$. A calculation of the centroid of the distribution of $\boldsymbol{v} \cdot \boldsymbol{E}_r$ yields the amplifying factor $A_w = \delta_w/\delta_-^H$. The theory of weak measurement is schematically shown in Fig. 3(a).

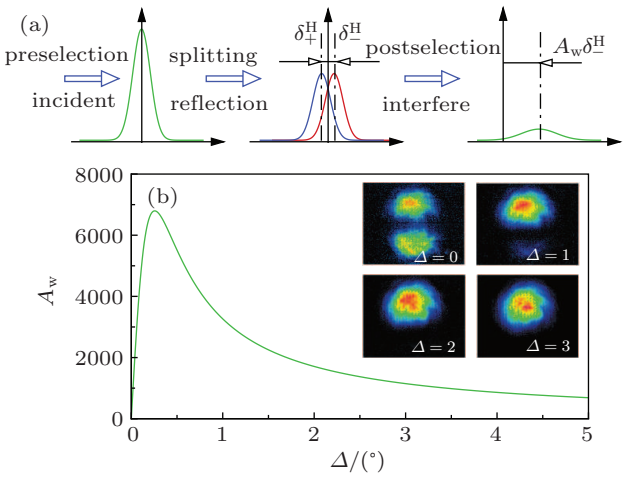


Fig. 3. (color online) (a) Preselection and postselection of polarization gives rise to an interference in the CCD, and shifts it to its final centroid position proportional to $A_w = \delta_w/\delta_-^H$. (b) Amplifying factor versus the postselected polarization angle Δ. Inset presents the field distributions for several postselected polarization angles. The beam waist of the incident beam is $w_0 = 18.66$ μm, and the incident angle is chosen as $\theta_i = 60°$.

We now determine an appropriate postselected polarization state in weak measurements. Figure 3(b) shows the amplifying factor versus the postselected polarization angle Δ. The amplifying factor first increases and reaches its maximum at $\Delta = 0.26°$, then decreases with the increase of Δ. In addition, we measure the field distributions for several postselected polarization angles (see inset of Fig. 3(b)). If the postselected polarization angle is at $\Delta = 0°$ exactly, the initial field component (H-polarization) is perfectly suppressed, and only the cross polarized component (V-polarization) is measured. Note that this interesting cross-polarization effect also can be observed in propagation.[23,24] In the case of $\Delta = 0°$, the amplifying factor $A_w = 0$, and no amplifying transverse displacement of the field centroid is detected. For a small value of Δ, the detected power is about 10 nw, and the measurability of very small displacements is limited by the electronic noise in the CCD. To improve the detected power, we choose $\Delta = 2 \pm 0.04°$ in the following measurements.

Figure 4 shows the original displacements, the amplified displacements, and the amplifying factors versus the incident angle. For the uniaxial crystal, the Brewster angle can be varied by rotating the optical axis, as shown in Figs. 4(a) and 4(b). At $\varphi = 0°$, the displacements of left-circularly and right-circularly polarized spin components increase with the increasing θ_i and change rapidly when θ_i is approaching the Brewster angle θ_B ($\sim 62.6°$). When $\theta_i > \theta_B$, the displacements of left-circularly and right-circularly polarized spin components shift oppositely, and decrease with the increasing θ_i (Fig. 4(a)). At $\varphi = 90°$, the change trend is the same as the former case, while its Brewster angle is $\theta_B = \sim 66.4°$ (Fig. 4(b)). In order to investigate how to switch the directions of spin accumulation, we choose $\varphi = 0°$ and $\varphi = 90°$ as examples and measure the amplified displacements of the two cases. Our theoretical and experimental results for the amplified displacement versus θ_i are reported in Figs. 4(c) and 4(d). We measure the displacements every 0.5° from 58° to 68° at $\varphi = 0°$ and every 0.5° from 60° to 72° at $\varphi = 90°$ respectively. The experimental and theoretical results of the amplifying factor in the weak measurement versus θ_i are shown in Figs. 4(e) and 4(f). A valley near the Brewster angle on reflection is presented in both cases. The experimental data are in good agreement with the theory without the use of fit parameters.

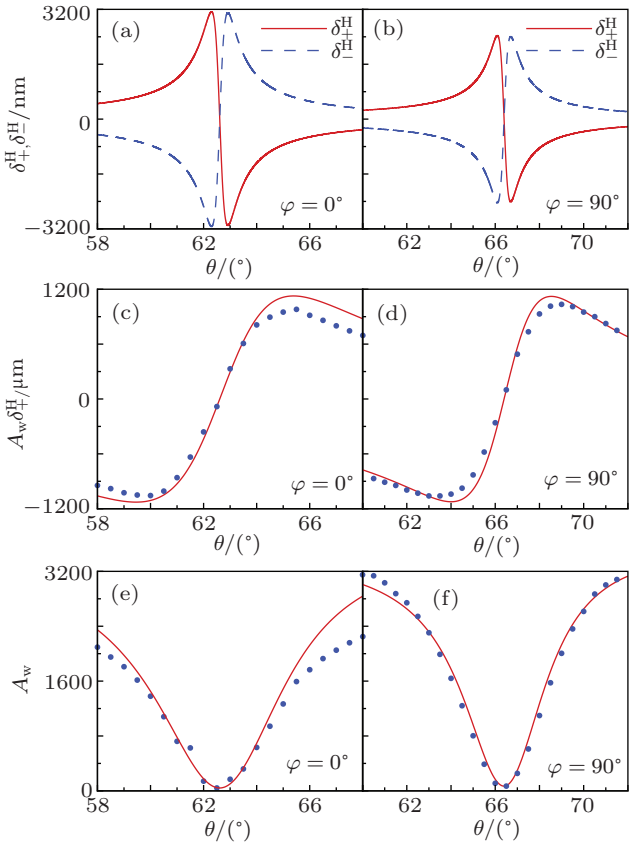


Fig. 4. (color online) Theoretical transverse displacements of left-circularly and right-circularly polarized spin components at the crystal interface each as a function of θ_i at (a) $\varphi = 0°$ and (b) $\varphi = 90°$. Theoretical and experimental results for amplified displacements versus θ_i in the case of (c) $\varphi = 0°$ and (d) $\varphi = 90°$. Theoretical and experimental results for amplifying factor A_w in the weak measurement for (g) $\varphi = 0°$ and (f) $\varphi = 90°$. The solid lines indicate the theoretical predictions, and the dots are the experimental data.

The signs of amplified shifts provide indirect evidence to determine the direction of spin accumulation of the SHE of light, since $\delta_{\rm w}$ has the same tendency as $\delta_{-}^{\rm H}$. Figure 5 shows the theoretical and experimental results for the amplified displacements and the measured field distributions. We can find that the directions of the amplified displacements are opposite at the same incident angle (Fig. 5(a)). This means that the spin accumulation reverses its direction when we rotate the optical axis. At the same incident angle $\theta_{\rm i} = 64°$, the amplified displacement is 882 μm for $\varphi = 0°$, while it is -1123 μm for $\varphi = 90°$. We also measure the field distributions at $\varphi = 0°$ and $\varphi = 90°$ for three different incident angles (Figs. 5(b)–5(g)). These intensity distributions show the deviations of the field centroid compared to the geometrical-optics prediction at different cases. When the incident angle $\theta_{\rm i}$ is in the range from 62.6° to 66.4°, the amplified displacement is positive at $\varphi = 0°$, while it is negative at $\varphi = 90°$. This means that the direction of photon accumulation can be reversed by adjusting the optical axis angle. This interesting characteristic is similar to the switching effect of spin accumulation in an electronic system.[25]

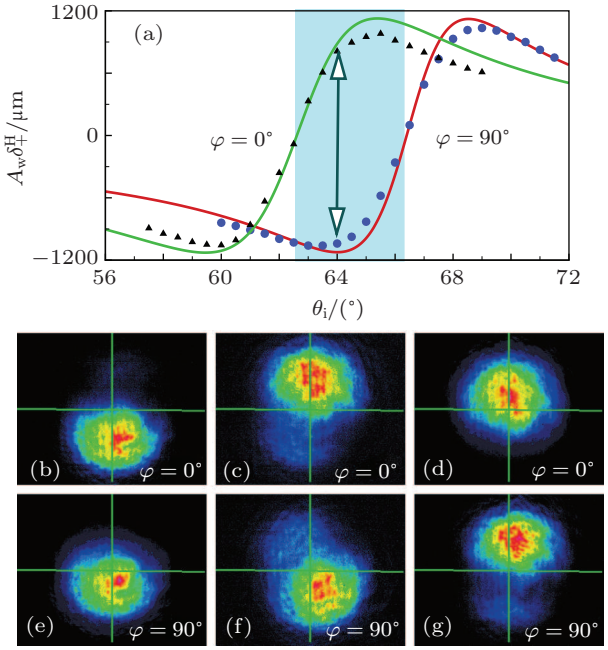


Fig. 5. (color online) (a) Theoretical and experimental results for amplified displacements versus $\theta_{\rm i}$. The red line and blue spots indicate theoretical and experimental results for amplified displacements at $\varphi = 90°$, respectively. The green line and the black triangles indicate theoretical and experimental results for amplified displacements at $\varphi = 0°$, respectively. The measured field distributions at $\varphi = 0°$ (first row) and $\varphi = 90°$ (second row) for different incident angles ((b), (e) $\theta_{\rm i} = 60°$; (c), (f) $\theta_{\rm i} = 64°$; (d), (g) $\theta_{\rm i} = 68°$) are also given.

4. Conclusion

In conclusion, we have presented theoretical and experimental research on a switchable SHE of light when a beam is reflected near the Brewster angle at an air–uniaxial crystal interface. We have found a large transverse spin splitting near the Brewster angle, whose sign can be altered by rotating the optical axis. As an analogy of the SHE in an electronic system, a switchable spin accumulation in the SHE of light is detected. We are able to switch the directions of the spin accumulation by adjusting the optical axis angle of the uniaxial crystal. It is expected that the SHE of light in an uniaxial crystal will be useful for nano-photonic devices, for example, by replacing the uniaxial crystal with a nematic liquid crystal whose optical axis can be tuned by an electric field.[26]

References

[1] Onoda M, Murakami S and Nagaosa N 2004 *Phys. Rev. Lett.* **93** 083901
[2] Bliokh K Y and Bliokh Y P 2006 *Phys. Rev. Lett.* **96** 073903
[3] Hosten O and Kwiat P 2008 *Science.* **319** 787
[4] Gosselin P, Bérard A and Mohrbach H 2007 *Phys. Rev. D* **75** 084035
[5] Aiello A and Woerdman J P 2008 *Opt. Lett.* **33** 1437
[6] Aiello A, Lindlein N, Marquardt C and Leuchs G 2009 *Phys. Rev. Lett.* **103** 100401
[7] Luo H, Wen S, Shu W, Tang Z, Zou Y and Fan D 2009 *Phys. Rev. A* **80** 043810
[8] Luo H, Ling X, Shu W, Wen S and Fan D 2011 *Phys. Rev. A* **84** 033801
[9] Tang M, Zhou X, Luo H and Wen S 2012 *Chin. Phys. B* **21** 124201
[10] Gorodetski Y, Niv A, Kleiner V and Hasman E 2008 *Phys. Rev. Lett.* **101** 043903
[11] Bliokh K Y, Niv A, Kleiner V and Hasman E 2008 *Nat. Photonics.* **2** 748
[12] Haefner D, Sukhov S and Dogariu A 2009 *Phys. Rev. Lett.* **102** 123903
[13] Qin Y, Li Y, He H Y and Gong Q H 2009 *Opt. Lett.* **34** 2551
[14] Rodríguez-Herrera O G, Lara D, Bliokh K Y, Ostrovskaya E A and Dainty C 2010 *Phys. Rev. Lett.* **104** 253601
[15] Qin Y, Li Y, Feng X, Liu Z, He H, Xiao Y and Gong Q 2010 *Opt. Express* **18** 16832
[16] Ménard J, Mattacchione A E, Vandriel Hautmann H M C and Betz M 2010 *Phys. Rev. B* **82** 045303
[17] Zhou X, Xiao Z, Luo H and Wen S 2012 *Phys. Rev. A* **85** 043809
[18] Leyder C, Romanelli M, Karr J P, Giacobino E, Liew T C H, Glazov M M, Kavokin A V, Malpuech G and Bramati A 2007 *Nat. Phys.* **3** 628
[19] Luo H, Zhou X, Wen S, Shu W and Fan D 2011 *Phys. Rev. A* **84** 043806
[20] Beth R A 1936 *Phys. Rev.* **50** 115
[21] Aharonov Y, Albert D Z and Vaidman L 1988 *Phys. Rev. Lett.* **60** 1351
[22] Ritchie N W M, Story J G and Hulet R G 1991 *Phys. Rev. Lett.* **66** 1107
[23] Ciattoni A, Crosignani B and Porto P Di 2001 *J. Opt. Soc. Am. A* **18** 1656
[24] Ciattoni A and Palma C 2003 *J. Opt. Soc. Am. A* **20** 2163
[25] Ando Y, Maeda Y, Kasahara K, Yamada S, Masaki K, Hoshi Y, Sawano K, Izunome K, Sakai A, Miyao M and Hamaya K 2011 *Appl. Phys. Lett.* **99** 132511
[26] Pishnyak O P and Lavrentovich O D 2006 *Appl. Phys. Lett.* **89** 251103